

Programmable Solid State Atom Sources for Nanofabrication

Electronic Supplementary Information

Han Han, Matthias Imboden, Thomas Stark, Pablo G. del Corro, Flavio Pardo, Cristian A. Bolle,
Lally W. Richard and David J. Bishop

Contents

S1. Thermal deformation and voltage sweep of the source.....	2
S2. Failure of the Al ₂ O ₃ coating on the source.....	3
S3. Summary of selected evaporations of eight different metals	6
S4. Using the micro source as a calorimeter.....	7
S5. Frequency stability of the mass-sensing resonator in a cryostat.....	11
S6. SEM images of sources with evaporating metal	13

S1. Thermal deformation and voltage sweep of the source

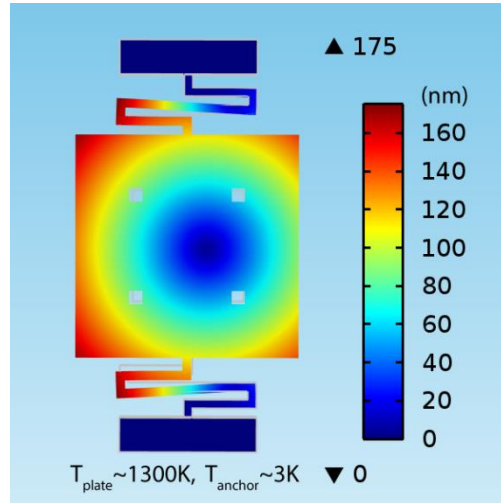


Figure S1. Finite element simulation of the mechanical deformation due to thermal expansion of the source. Color scale shows displacement in nanometers with the source plate heated to 1300 K and the anchors at 3K. The deformation in the figure is exaggerated. The spring shaped heaters allow the structure to bend, ensuring the mechanical integrity of the device during hundreds of thermal cycles.

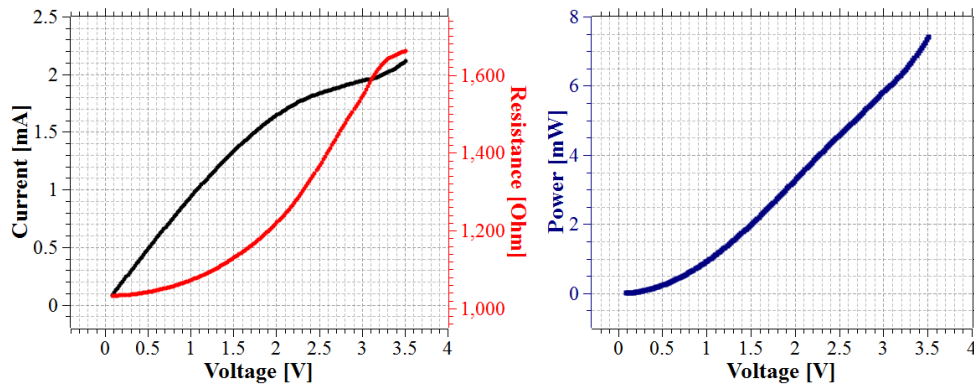


Figure S2. Voltage sweep of the unloaded MEMS source. When the voltage exceeds 3 V (point of inflection), the source becomes unstable. This can be explained by thermal breakdown of the polysilicon or other possible causes.¹

S2. Failure of the Al₂O₃ coating on the source

As described in the main text, the Al₂O₃ coating helps by separating the polysilicon structure and the loaded material to prevent silicide formation which will greatly degrade the source's performance and eventually break the heater. After an extended use of the source, especially at high working temperature, defects start to occur on the sapphire that can expose the polysilicon to the material thus make the entire source fail. Figure S3 shows three SEM images of a source being actuated with 100 ms pulses. It can be observed that the defects in the form of pitting gradually show up in the center of the source plate as the pulse power is ramped up above 8.75 mW. When metal is present, such defects will allow the metal to react with the polysilicon. Figure S4 demonstrates the failure process of a source loaded with gold. The source was actuated with 100 ms ~9.0 mW constant voltage pulses. The defect slowly developed in this case and allowed gold to diffuse into the polysilicon source plate. The silicide formation eventually reached the joint where the heater connects to the plate, breaking the source at this weak link. For a source without the protective shadow mask, the failure could happen even earlier because the serpentine heater is more vulnerable to silicide formation as discussed in the main text: it experiences stronger thermal stresses and higher temperatures. Figure S5 shows a burnt heater with lead on it. The shattered Al₂O₃ layer is still visible in the close-up.

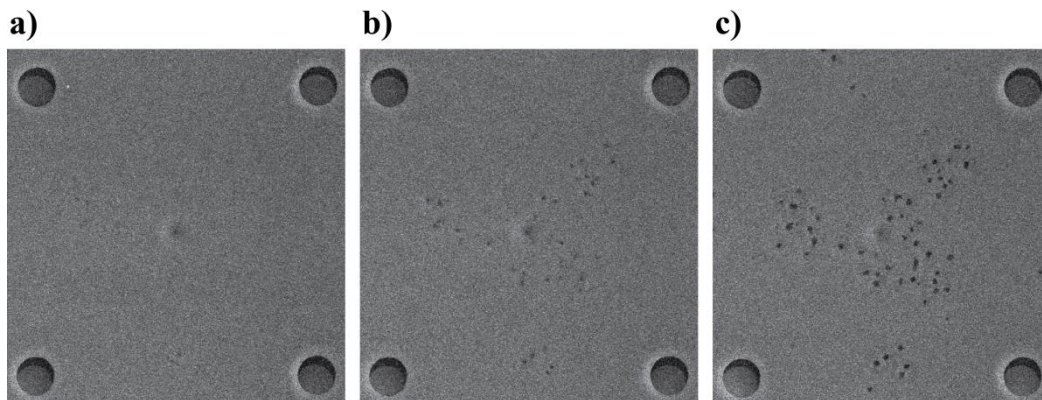


Figure S3. Three SEM images of a source being pulsed to high temperature. The silver on the source plate got depleted in image (a), when the power is 8.31 mW. In image (b), pitting starts to be visible at 8.75 mW. In image (c) the power will not go higher even with a higher voltage pulse because the polysilicon structure is damaged as defects become severer.

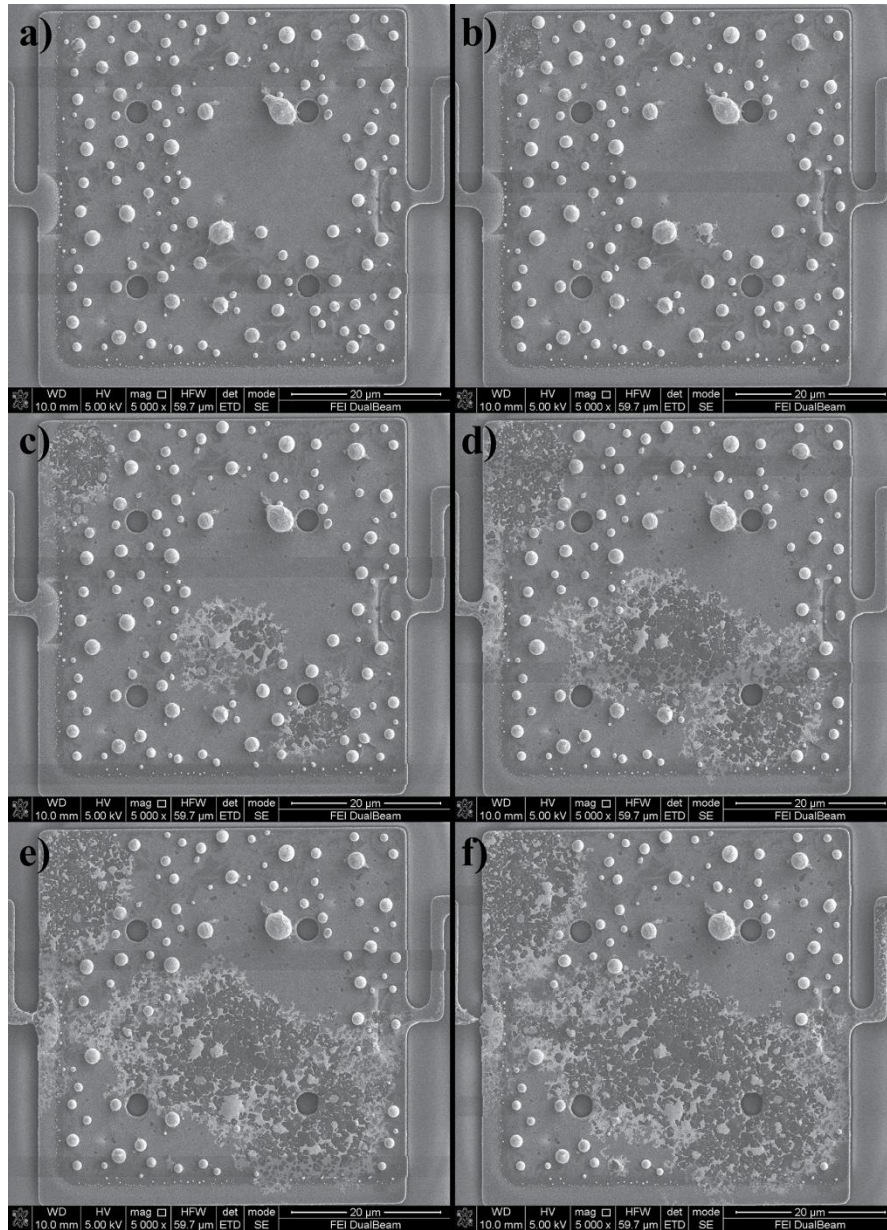


Figure S4. The failure process of a source loaded with gold observed in an SEM. The defect opened up the polysilicon to gold thus silicide started to form. Eventually the reaction broke the joint between the source plate and left heater.

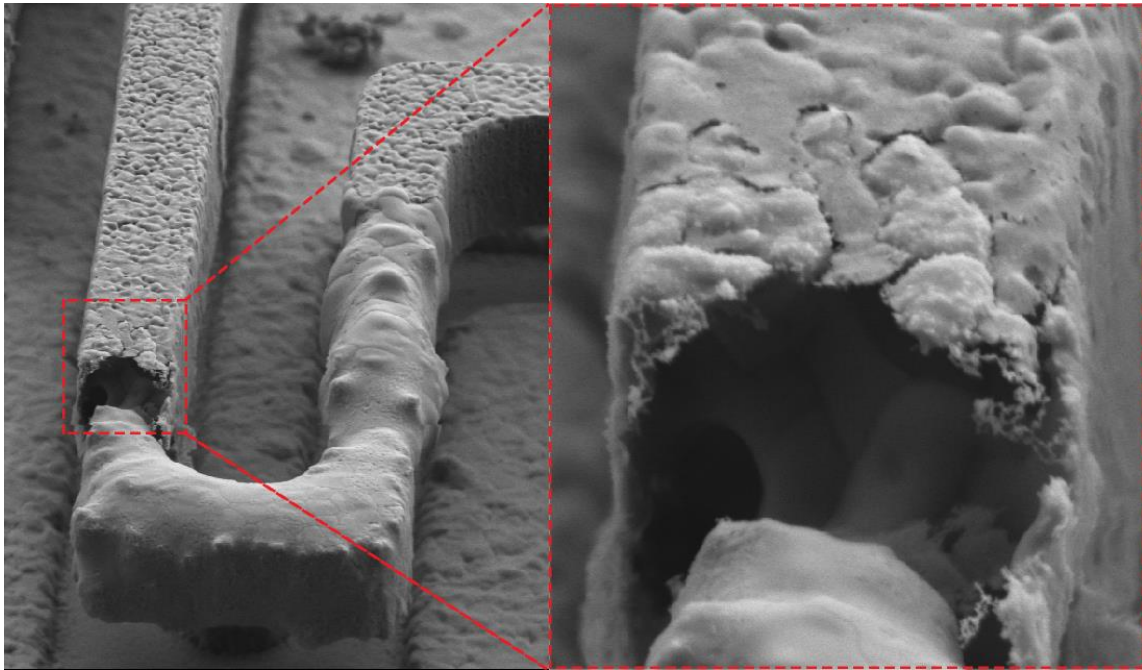


Figure S5. A failed heater element with lead. The heater was not protected by the micro shadow mask so that lead was deposited on it during evaporant loading. The shattered Al₂O₃ layer can be seen on the zoom-in image.

S3. Summary of selected evaporations of eight different metals

Metal	Metal thickness [nm]	Device thickness [μm]	Base Temp. [K]	Pulsed Power [mW]	Pulse Width [ms]	Source Resistance during pulse [Ohm]	Heat Input [mJ]	Frequency Shift [mHz]
Ag	60	1.5	300	6.39	52,000	3175	332	3340 \pm 33
Pb	120	1.5	300	3.10	29,000	1289	90.0	2630 \pm 70
Au	100	2.0	300	4.69	436,000	1350	2020	390 \pm 36
Fe	25	2.0	300	4.49	67,000	1507	301	59 \pm 9
Al	100	2.0	300	4.10	13,000	1290	53.3	132 \pm 6
Cu	50	2.0	300	7.59	100	960	0.759	169 \pm 10
Sn	50	1.5	300	2.88	472,000	2167	1360	742 \pm 21
In	60	1.5	300	3.84	5,000	2662	19.2	2942 \pm 75
In	150	1.5	300	3.04	53,000	3370	161	8099 \pm 123
In	120	1.5	3	5.98	10	1931	0.0598	0.0157 \pm 0.0011
In	120	1.5	3	5.79	20	1997	0.116	0.221 \pm 0.048
In	120	1.5	3	6.01	100	2036	0.601	1.39 \pm 0.08

Table S1. Parameters of typical evaporations of different materials, using the 50 μm \times 50 μm sources. Two variations of the source with different polysilicon thickness were used. The data is depicted in Figure 6 of the main text.

S4. Using the micro source as a calorimeter

The resistance measurement on the source during a pulse provides important information about the thermal properties of the source and the material on it. When the source is being pulsed, heat is generated in the heaters and flows to the source plate. The elevated temperature will cause an increase in the resistance (as seen in Figure S2) and is described in Ref [1]. For a voltage biased system the rising resistance will reduce the power, where a current bias may lead to runaway heating. Eventually, the source will reach equilibrium and the temperature and resistance remain constant, as the power generated from joule heating is equal to the total heat dissipation through radiation and thermal conduction to the anchor. Given the fact that the resistance monotonically increases with temperature (within the range we are interested in), the resistance can be used as a scale of the temperature. By pulsing the source many times with different voltages, one can map out the relationship between equilibrium power and resistance. The heat dissipation at a given resistance can then be extrapolated from the measured power-resistance data. The power-resistance relation is plotted in Figure S6 and a linear fitting describes the relationship well within the range we care about. As discussed in the main text, the silver melting effect emerges when the pulsed voltage reaches around 6.7 V. Figure S7 plotted the resistance on the rising edges of three different voltages pulses. What can be seen is that for 6680 mV there is no melting-induced resistance plateau on the curve, while for slightly higher pulses at 6730 mV and 6780 mV the plateau appears. For the two higher voltage pulses, the power is sufficient for the source to reach the melting temperature of the loaded silver. As it melts the material will consume heat and undergo a phase transition (this is the latent heat of melting). This power drain will prevent the temperature of the whole source plate from increasing, until the melting is completed. After the melting procedure finished, the resistance will resume ramping up until equilibrium is reached. The total thermal energy absorbed by the silver is equal to the product of its mass and its latent heat per unit mass. This must equal to the time integral of power difference between heat generated from joule heating (power in) and the heat dissipation (power out) which can be estimated using the method discussed earlier.

$$P_{Ag} = P_{Joule} - P_{dissipation} = \frac{V_{pulse}^2}{R} - P_{dissipation}(R) \quad (S1)$$

where P_{Ag} is the power consumption of silver melting. Once melting finishes and the equilibrium is established again, the heating power will be equal to the dissipation:

$$P_{dissipation}(R_{eq}) = \frac{V_{pulse}^2}{R_{eq}} \quad (S2)$$

Recalling that the dissipation is linearly related to the resistance, this will lead to:

$$P_{Ag} = V_{pulse}^2 \left(\frac{1}{R} - \frac{1}{R_{eq}} \right) + b(R_{eq} - R) \quad (S3)$$

where b is the slope of the linear fit on the heat dissipation data in Figure S6, and $b \approx (1.08 \pm 0.01) \times 10^{-5} \text{ W}/\Omega$. Here we assume that the linear relationship between dissipation and resistance remains during the phase transition of the loaded material because as discussed in the main text thermal conduction through the polysilicon heaters is the dominated mode of dissipation and will not be affected by the state of loaded material. Therefore, by integrating both sides over time, we get:

$$m_{Ag} Q_{Ag} = \int \left[V_{pulse}^2 \left(\frac{1}{R} - \frac{1}{R_{eq}} \right) + b(R_{eq} - R) \right] dt. \quad (S4)$$

Q_{Ag} is the specific latent heat of silver melting. The mass of material m_{Ag} can be calculated based on its thickness and the receiving area of the source plate. The integral on the right can be computed from the resistance data in Figure S7. By performing this calculation on the data from 6730 mV pulse, the latent heat is estimated to be $70 \pm 20 \text{ kJ/kg}$, while the referenced value is 88 kJ/kg . This result validates the hypothesis of material melting and the discrepancy of the latent heat value can be explained by the uncertainty of the film thickness loaded on the source. This phenomenon is observed in a FEM simulation as well, which is shown in Figure S8.

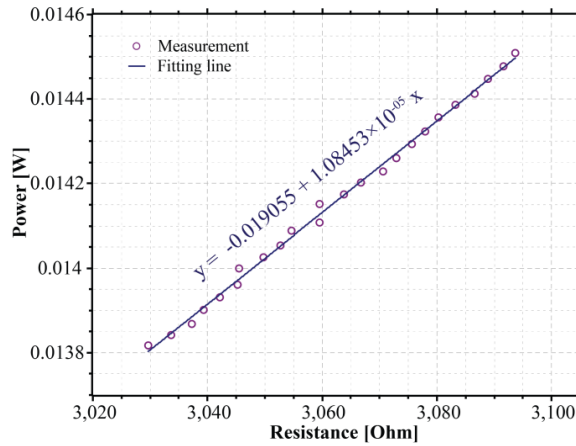


Figure S6. Measured power-resistance data at equilibrium, when the applied power is equal to total dissipation. A fit suggests an empirical linear relationship between heat dissipation and source resistance.

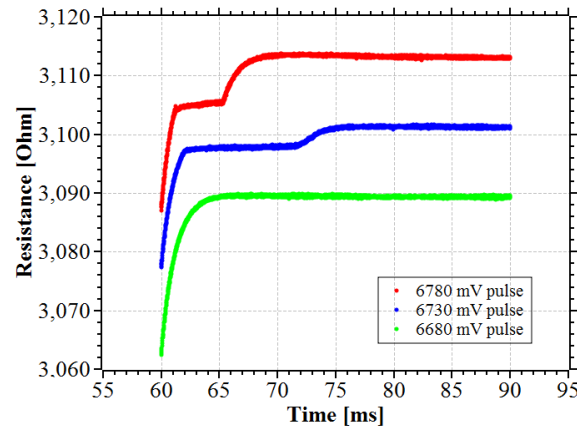


Figure S7. Resistance plots on the rising edges of three pulses at different voltages. At 6680 mV no melting is observed, while at 6730 mV and 6780 mV the melting-induced resistance plateau is clearly visible. The 6780 mV pulse has a shorter melting duration since it provides more power that can be consumed by material melting.

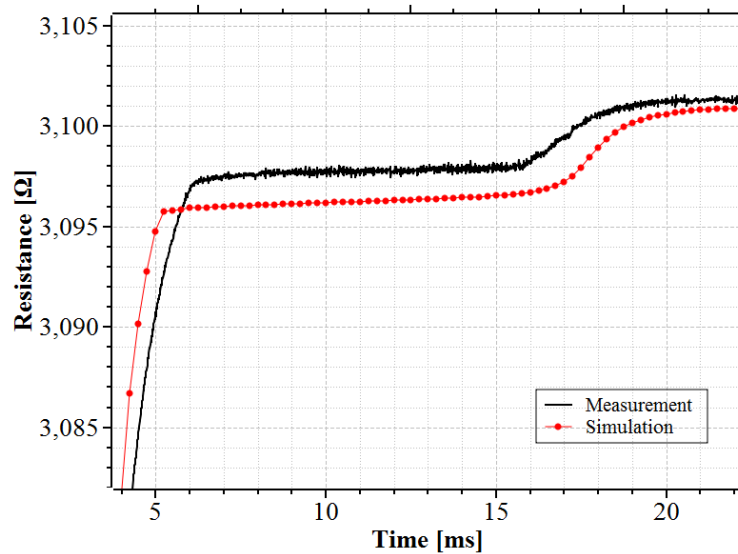


Figure S8. The FEM simulation shows a similar constant temperature plateau as in the measurement data. The x-axis for the simulation is shifted to match the time of melting. Before and after the melting time, the resistance exponentially approaches the equilibrium value.

The finite element simulation was matched to the experiment by adjusting the material properties of the polysilicon. As a baseline the following parameters were used: The temperature dependent resistivity was measured by [2] and [3], specifically for PolyMUMPs polysilicon; the thermal conductivity was taken from references [4] and [3]; and the references [5] and [6] contain data for the heat capacity and coefficient of thermal expansion of silicon. The temperature range of interest exceeds the range documented in the references, hence for 800 to 1500 Kelvin, the resistivity and thermal conductivity have been extrapolated based on the lower temperature measurements. It is assumed that the heat capacity of silicon is a good approximation to the doped polysilicon used in our experiments, this may not be an accurate assumption as the time axis had to be shifted for the simulation to match the experiment, indicating a higher than expected heat capacity. As tabulated on the MEMSCAP website⁷, the electrical conductivity can change considerable from run to run, so it should be assumed that the charge carriers will also affect the thermal conductivity.

Differences between the experimental response and simulations are expected, especially as the material properties are not known very precisely. To match both, the electrical and thermal conductivity were adjusted. The melting point of silver was used as a calibration value. It is known experimentally how much power must be applied to heat the samples. The plateau is an excellent indication of the sample temperature. In order for the simulation and experiment to match, the electrical resistivity was scaled by 5.3% (for all temperature values) and the

thermal conductivity was increased by a factor of 1.967. The resulting agreement can be seen in Figure S8. The electrical resistivity was scaled so that the simulation and experiment matched at the melting point of silver. The thermal conductivity was matched so that the total thermal energy dissipation matched the power input used in the experiment. The melting time of the silver is very sensitive to these properties, the qualitative agreement is however easily recovered.

The correction factor of the electrical resistivity is small and well within the variations expected from the PolyMUMSs fabrication runs. The relatively large correction of the thermal conductivity needed to match the simulations to the data is less easily explained. A significant contribution may be from differences in our actual material compared to the previously reported values.

S5. Frequency stability of the mass-sensing resonator in a cryostat

In order to detect the evaporation beyond the mass resolution of the resonator, the source is pulsed hundreds of times. This accumulates the mass loading effect while minimizing the thermal disturbances. Such a procedure can take an extended amount of time and requires the resonance frequency to be free of drifting or at least the drift must be predictable during the time when an evaporation-induced frequency shift is also present. By performing a background subtraction of the known drift, the evaporation-induced frequency shift can be extracted, as plotted in Figure 5(b) of the main text.

This experiment was conducted in a cryostat at around 3 K. Before the evaporation takes place, the resonance frequency is measured for 6000 seconds to study the stability. Such a measurement is plotted in Figure S9. A linear frequency drift is observed, which is caused by mass-loading from the gas molecule condensation on the resonator (improving the vacuum would eliminate this). Since the sample is cooled down to ~ 3 K, residual gas molecule in the chamber will condense on cold surfaces. It should be noted that the observed drift corresponds to the order of one monolayer of nitrogen every four hours. This drift is both slow and constant as the pressure of the vacuum chamber will reach a dynamic balance as condensation continues and new molecules leak in. It is shown that a linear fit can predict the frequency shift with an error less than 0.4 mHz, within the measurement period. The fit is used for background subtraction for the result in Figure 5(b) of the main text.

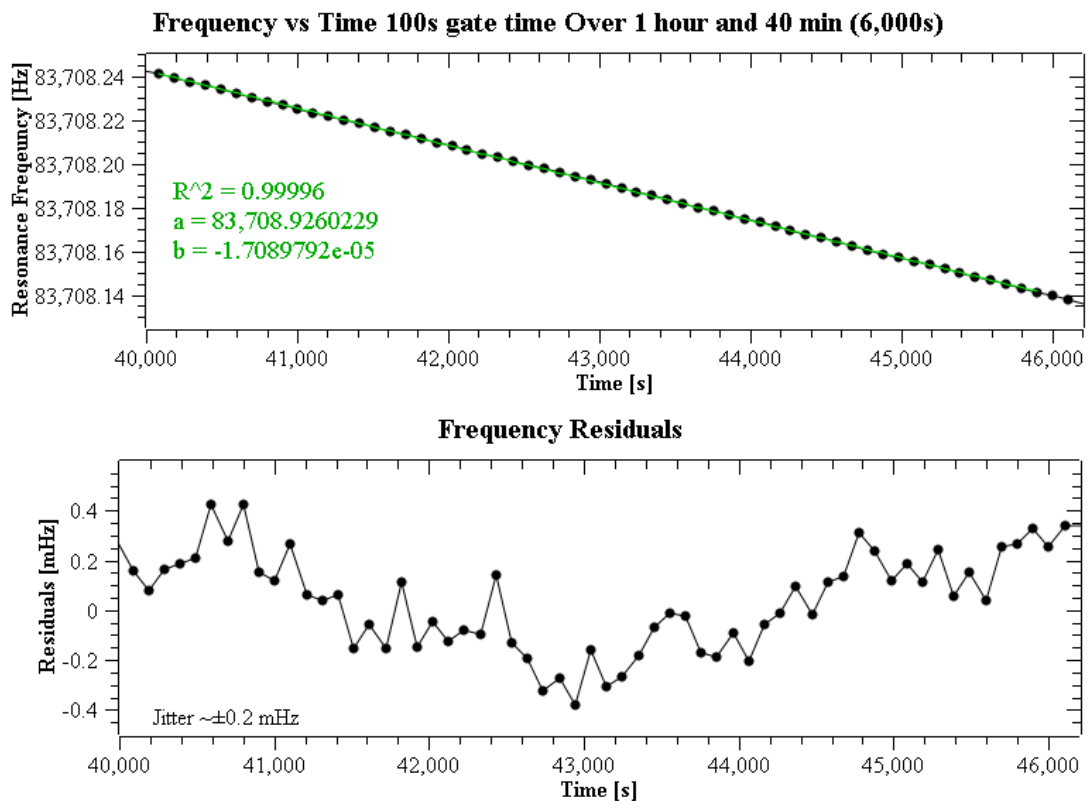


Figure S9. The frequency stability measurement for a resonator. The frequency was measured at a gate time of 100s, showing a linear background drifting, which is believed to be caused by mass-loading from gas molecule deposition. The frequency residual obtained by subtracting the data from the fitting line are below 0.4 mHz, showing that a linear fit is a good model to predict the frequency drift.

S6. SEM images of sources with evaporating metal

The evaporation process has been imaged in real time using SEM. In such an experiment, the sources were loaded with a desired metal and actuated inside an SEM chamber. The source plates were then pulsed hundreds of times while the SEM took an image after each pulse. Figure S10 shows selected images from the data set of a source loaded initially with 150 nm of silver. The corresponding video constructed from the SEM images can be found in the online Electronic Supplementary Information. In this experiment the source element was pulsed 230 times. Pulses started at 1 V and were incremented by 10 mV each time until the maximum pulse amplitude of 3.3 V was reached, by when all source material had evaporated. It can be seen that as the power increases the silver film changed its roughness, then melted and balled up, and eventually evaporated to depletion. In a common setup the target is facing the source with both surface in parallel, and the sizes of both target and source are relatively small compared to their distance, so that we only care about the deposition flux in the normal direction of the target plane. The deposition flux on the target is proportional to the projected area of the evaporant's surface in the normal direction. As the material gets evaporated off, the morphology changes and the surface area shrinks. This effect can be seen in the SEM images taken as described above. We care about the flux at the normal direction of the target plane, which is proportional to the projected surface area of silver on the 2D plane parallel to the source plate. This is exactly what has been captured in the SEM images.

The projected surface area can be quantitatively estimated by utilizing an image processing algorithm on the SEM images. The evaporant and polysilicon plate have very different contrasts as viewed in an SEM. Hence the sum of gray scale value of each pixel within the source plate area provides a measure of how much area of the source plate is covered by metal. Figure S11 shows the pixel values of a silver grain and its surrounding area of bare polysilicon source plate. The image's contrast and brightness have been adjusted so that metal and polysilicon can be better distinguished. For a given image during the evaporation, the summation over the plate is subtracted by the image of an empty source plate as a background. The value is then normalized to a range from 0 to 1, by setting the first image when entire plate is uniformly covered to be 1. This normalized value can be regarded as a relative projected area of the evaporant. It should be noted again that this measure can only map out the surface area projected on the normal direction, while not counting the area of the curved side wall of the metal grain resulting from dewetting. However, since the target is typically placed facing the normal direction of the source, the projected surface area is an accurate measure to estimate the evaporation flux in this direction. For a constant temperature, the deposition flux in the normal direction of the target plane is proportional to the surface area of the evaporant projected onto that direction.

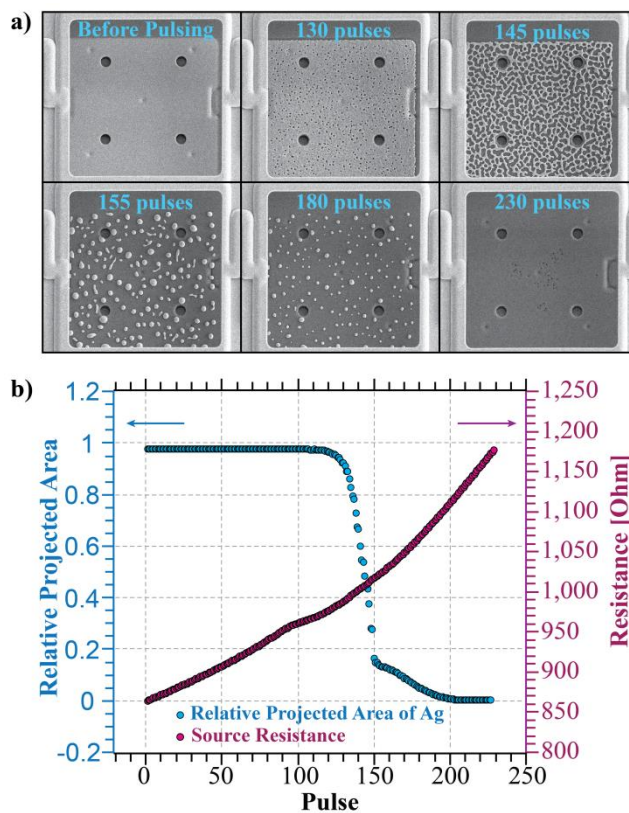


Figure S10. A source loaded with 150 nm of silver was pulsed 230 times. Pulse amplitudes were swept from 1 V to 3.3 V in 10 mV increments. a) Six SEM images during the pulses. Before pulsing, the source was covered uniformly with silver. As the pulse power increased silver started to melt and evaporate, resulting in a decrease of projected surface area. Eventually all the silver is depleted. b) The resistance of the source increased at higher temperature resulting from higher pulse powers. The projected surface area covered by silver was determined using the intensity of the SEM images and is plotted on the same graph.

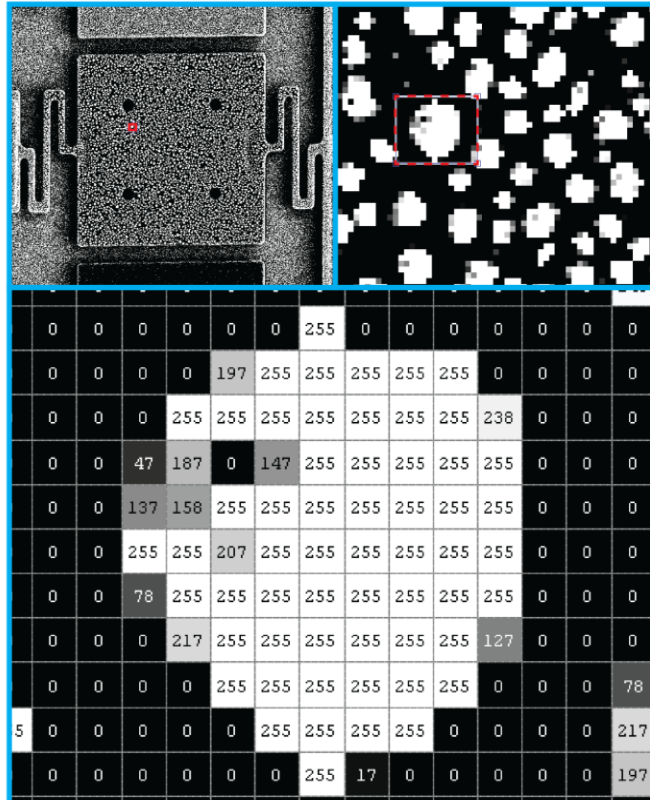


Figure S11. SEM image of a source evaporating Indium. Upon melting the metal balled up to many small grains and the projected surface area is measured by summing up the pixel values. The bottom figure shows the pixel values are for a very small region containing a single metal grain.

Reference

- 1 C. H. Mastrangelo, J.-J. Yeh and R. S. Muller, *Electron Devices, IEEE Trans.*, 1992, **39**, 1363–1375.
- 2 M. Imboden, H. Han, T. Stark, E. Lowell, J. Chang, F. Pardo, C. Bolle, P. G. del Corro and D. J. Bishop, *Nanoscale*, 2014, **6**, 5049–62.
- 3 A. A. Geisberger, N. Sarkar, M. Ellis and G. D. Skidmore, *J. Microelectromechanical Syst.*, 2003, **12**, 513–523.
- 4 A. D. McConnell, S. Uma and K. E. Goodson, *J. Microelectromechanical Syst.*, 2001, **10**, 360–369.
- 5 P. D. Desai, *J. Phys. Chem. Ref. Data*, 1986, **15**, 967.
- 6 Y. Okada and Y. Tokumaru, *J. Appl. Phys.*, 1984, **56**, 314.
- 7 MEMSCAP, <http://www.memscap.com/products/mumps/polymumps/reference-material>.